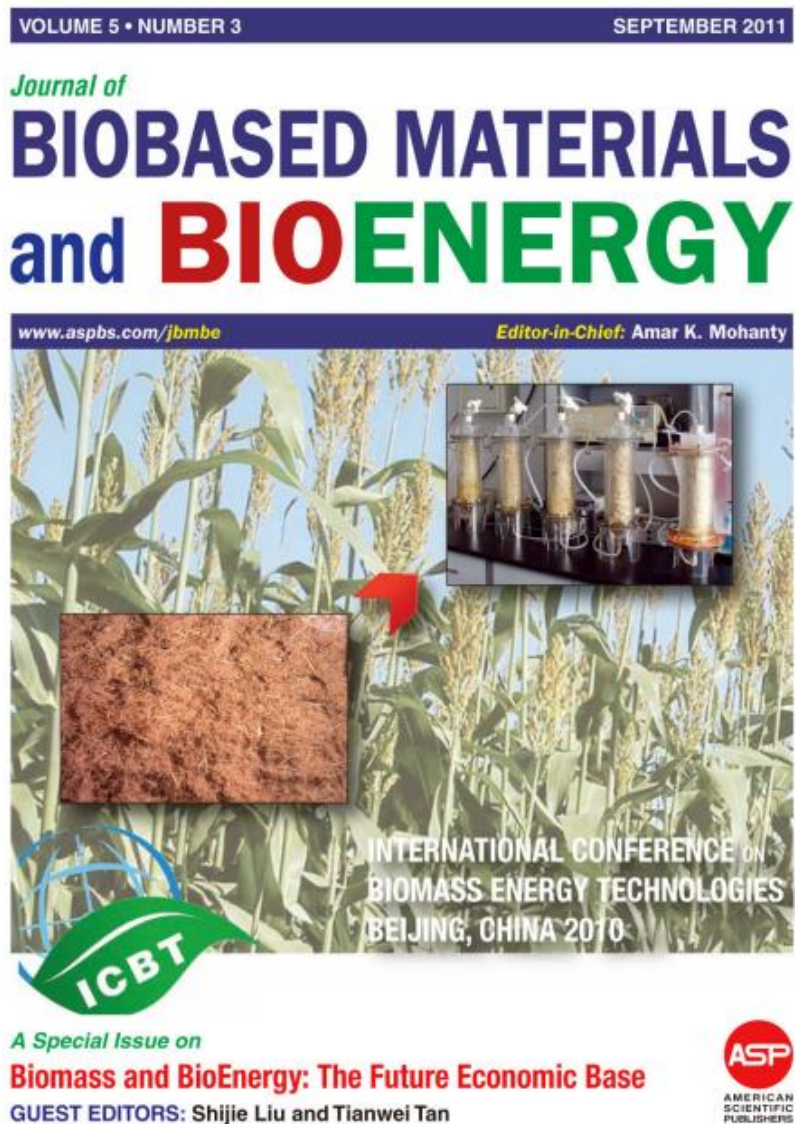


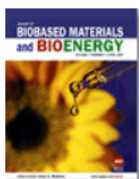
Paper 8 Not open access :

Thermal, Biodegradability and Water Barrier Properties of Bio-Nanocomposites Based on Plasticised Sugar Palm Starch and Nanofibrillated Celluloses from Sugar Palm Fibres

Silahkan klik google drive utk full access:

<https://drive.google.com/file/d/1KLttj1Ahsvs4wpbbC1D2A9CIJZ9xCeoH/view?usp=sharing>





Thermal, Biodegradability and Water Barrier Properties of Bio-Nanocomposites Based on Plasticised Sugar Palm Starch and Nanofibrillated Celluloses from Sugar Palm Fibres

Buy Article:

\$107.14 + tax
(Refund Policy)

[ADD TO CART](#)

[BUY NOW](#)

Authors: Ilyas, R. A.; Sapuan, S. M.; Ibrahim, Rushdan; Abrial, Hairul; Ishak, M. R.; Zainudin, E. S.; Atiqah, A.; Atikah, M. S. N.; Syafri, Edi; Asrofi, Mochamad; Jumaidin, R.

Source: Journal of Biobased Materials and Bioenergy, Volume 14, Number 2, April 2020, pp. 234-248(15)

Publisher: American Scientific Publishers



Journal of Biobased Materials and Bioenergy

ISSN: 1556-6560 (Print); EISSN: 1556-6579 (Online)
Copyright © 2000-2023 American Scientific Publishers. All Rights Reserved.

EDITORS-IN-CHIEF

Professor Shijie Liu

Department of Paper and Bioprocess Engineering
State University of New York
College of Environmental Science and Forestry (SUNY ESF)
1 Forestry Drive, Syracuse, New York 13210, USA
Email: sliu@esf.edu

Prof. Dr. Nongyue He

State Key Laboratory of Biological Electronics
School of Biological Science and Medical Engineering
Southeast University, Nanjing, 210096, P.R. China
Email: nyhe1958@163.com

EDITORS

Prof. Koon-Yang Lee

Department of Chemical Engineering
University College London, UK

Prof. Run-Cang Sun

College of Light Industry and Chemical Engineering
Dalian Polytechnic University, Dalian, China

Prof. Rodrigo Navia

University of La Frontera, Chile

Prof. Xiao-Feng Tan

Key Laboratory of Cultivation
& Protection for Non-Wood Forest Trees
Central South University Forestry and Technology, China

Prof. Zhu Long

School of Textiles and Clothing
Jiangnan University, China

Prof. Ding Li

Department of Biotechnology
Hunan University of Technology, China

EDITORIAL BOARD

Lars Berglund, Royal Institute of Technology, Sweden
Debes Bhattacharyya, University of Auckland, New Zealand
Girma Biresaw, USDAARS, NCAUR, Peoria, IL, USA
John P. Buyondo, International Flavors & Fragrances, Rochester, USA
Kenneth G. Cassman, University of Nebraska, Lincoln, Nebraska, USA
K. Chandrashekhara, Missouri University of Science and Technology, USA
Jonathan Chen, The University of Texas at Austin, USA
Jorge Luiz Colodett, Universidade Federal de Vicosa (UFV), Brazil
Ajay K. Dalai, University of Saskatchewan, Saskatoon, Canada
Yulin Deng, School of Chemical & Biomolecular Engineering, Georgia Tech. USA
Lawrence T. Drzal, Michigan State University, East Lansing, Michigan, USA
Gregory Joseph Duns, Nanjing Technical University, China
Stephen Eichhorn, University of Manchester, UK
Gregory M. Glenn, USDA, ARS, Western Regional Research Center, Albany, CA, USA
Bruce Harte, Michigan State University, East Lansing, Michigan, USA
Mikael Hedenqvist, Royal Institute of Technology, Sweden
Adriaan van Heiningen, University of Maine, Orono, Maine, USA
Jörg Müssig, Hochschule Bremen, University of Applied Sciences, Germany
Alma Hodzic, University of Sheffield, UK
Tadahisa Iwata, The University of Tokyo, Japan
Raghavan Jayaraman, University of Manitoba, Winnipeg, Canada
Jianxin Jiang, Beijing Forestry University, China
George John, The City College of New York, The City University of New York, USA
Hyun-Joong Kim, Seoul National University, Seoul, Korea
Marie-Pierre Laborie, Albert-Ludwigs University of Freiburg, Freiburg, Germany
Richard C. Larock, Iowa State University, Ames, Iowa, USA
Bin Liang, Sichuan University, Chengdu, China
Lu Lin, Xiamen University, Fujian Province, China
Dehuan Liu, Tsinghua University, Beijing, China
Guangqing Liu, Beijing University of Chemical Technology, Beijing, China
LinShu Liu, USDA, ARS, Eastern Regional Research Center, USA
Naushad Mu, King Saud University, Riyadh, Kingdom of Saudi Arabia
Ramani Narayan, Michigan State University, East Lansing, USA
Anil N. Netravali, College of Human Ecology, Cornell University, USA
Xuejun Pan, University of Wisconsin-Madison, USA
Satyanarayan Panigrahi, University of Saskatchewan, Saskatoon, Canada
Martin Patel, Utrecht University, The Netherland
Ton Peijs, Queen Mary, University of London, UK
Arthur J. Ragauskas, University of Tennessee, USA
Kurt A. Rosentrater, Iowa State University, USA
Badal C. Saha, National Center for Agricultural Utilization Research (NCAUR), USDA-ARS, USA
Mohini Mohan Sain, University of Toronto, Canada
Gordon Selling, USDA-ARS-NCAUR, Peoria, IL, USA
X. Susan Sun, Kansas State University, USA
Zhaohui Tong, University of Florida, Gainesville, USA
Lih-Shena Turna, University of Wisconsin-Madison, USA

Journal of Biobased Materials and Bioenergy

ISSN: 1556-6560 (Print); EISSN: 1556-6579 (Online)

Copyright © 2000-2023 American Scientific Publishers. All Rights Reserved.

Abstracting and Indexing

- Science Citation Index-Expanded (SCIE/SciSearch)
- Web of Science (WoS)
- Current Contents Engineering, Computing & Technology
- Essential Science Indicators
- ISI-Scientific Database
- Journal Citation Reports/Science Edition
- Materials Science Citation Index
- Chemical Abstracts Service (CAS)
- SciFinder
- Google Scholar

Terindeks WOS

The screenshot shows a web browser window displaying the search results for 'Journal of Biobased Materials and Bioenergy' on the Web of Science platform. The browser's address bar shows the URL 'mjl.clarivate.com/search-results'. The page features a navigation bar with 'Master Journal List', 'Search Journals', 'Match Manuscript', 'Downloads', and 'Help Center'. A blue banner at the top of the page reads 'The power of the Web of Science™ on your mobile device, wherever inspiration strikes.' Below this, there is a search bar containing the journal title and a 'Search' button. To the right of the search bar, there is a 'Sort By:' dropdown menu set to 'Relevancy'. The search results section indicates 'Found 860 results (Page 1)' and includes a 'Share These Results' link. Under the heading 'Exact Match Found', the journal's details are listed: 'PUBLISHER: AMER SCIENTIFIC PUBLISHERS, 26650 THE OLD RD, STE 208, VALENCIA, USA, CA, 91381-0751', 'ISSN / eISSN: 1556-6560 / 1556-6579', 'Web of Science Core Collection: Science Citation Index Expanded', and 'Additional Web of Science Indexes: Current Contents Engineering, Computing & Technology | Essential Science Indicators'. At the bottom of the results section, there are links for 'Share This Journal' and 'View profile page'. The browser's taskbar at the bottom shows the system tray with a temperature of 25°C, a battery level indicator, and the date 08/04/2023.

Journal of Biobased Materials and Bioenergy

Discontinued in Scopus as of 2017

COUNTRY

United States

 Universities and research institutions in United States

 Media Ranking in United States

SUBJECT AREA AND CATEGORY

Chemical Engineering
└ Bioengineering

Energy
└ Renewable Energy, Sustainability and the Environment

Materials Science
└ Biomaterials

PUBLISHER

American Scientific Publishers

H-INDEX

33

List of Contents

Thermal, Biodegradability and Water Barrier Properties of Bio-Nanocomposites Based on Plasticised Sugar Palm Starch and Nanofibrillated Celluloses from Sugar Palm Fibres

R. A. Ilyas, S. M. Sapuan, Rusdan Ibrahim, Hairul Abral, M. R. Ishak, E. S. Zainudin, A. Atiqah, M. S. N. Atikah, Edi Syafri, Mochamad Asrofi, and R. Jumaidin

J. Biobased Mater. Bioenergy 14, 234–248 (2020)

[\[Abstract\]](#) [\[Full Text - PDF\]](#) [\[Purchase Article\]](#)

Investigation of Multiple Pathogens in Black-Spotted *Dendrobium officinale* Based on Culture-Independent and Dependent Methods

Xiaoying Han, Yihong Dai, Miao Hu, Rong Xiao, Shuaishuai Zhang, Jin Li, Zhanqi Wang, Xiufang Hu, and Zhouhang Gu

J. Biobased Mater. Bioenergy 14, 249–257 (2020)

[\[Abstract\]](#) [\[Full Text - PDF\]](#) [\[Purchase Article\]](#)

Methane Production from *Pennisetum giganteum* z.x.lin During Anaerobic Digestion

Caiyan Liu, Baocheng Wei, Zhuangqiang Dai, Chang Chen, and Guangqing Liu

J. Biobased Mater. Bioenergy 14, 258–264 (2020)

[\[Abstract\]](#) [\[Full Text - PDF\]](#) [\[Purchase Article\]](#)

Pretreatment of Bamboo by Ammonium Sulfite for Efficient Enzymatic Hydrolysis

Liyue Zhang and Zhiqiang Li

J. Biobased Mater. Bioenergy 14, 265–272 (2020)

[\[Abstract\]](#) [\[Full Text - PDF\]](#) [\[Purchase Article\]](#)

Study on the Formation of Ethyl Levulinate from Wheat Straw Based on a Model Compound

Zhiyong Chen, Qian Guan, Haiyan Xu, Tingzhou Lei, Lu Lin, Zhiwei Wang, Xiaofeng He, and Jinling Zhu

J. Biobased Mater. Bioenergy 14, 273–279 (2020)

[\[Abstract\]](#) [\[Full Text - PDF\]](#) [\[Purchase Article\]](#)

The Treatment of Absorbable Organic Halogens and Organic Compounds in Simulated Bleaching Effluents Through the Response Surface Methodology Optimized Fenton System

Ming Lei, Qingtong Zhang, Douyong Min, and Shuangfei Wang

J. Biobased Mater. Bioenergy 14, 280–286 (2020)

[\[Abstract\]](#) [\[Full Text - PDF\]](#) [\[Purchase Article\]](#)

Screening and Characterization of Ethanol-Producing Yeasts from Sewage Sludge, Soil and Rotten Fruits

Chunming Wang, Xiaobing Chen, and Jialang Lao

J. Biobased Mater. Bioenergy 14, 287–293 (2020)

[\[Abstract\]](#) [\[Full Text - PDF\]](#) [\[Purchase Article\]](#)

Pervaporation Performance of Polydimethylsiloxane-Polyvinylidene Fluoride Composite Membrane for Butanol Recovery from Model Solutions and Acetone-Butanol-Ethanol Fermentation Broth

Yonghong Li, Jiping Shi, Xiaojie Liu, Qiang Yu, Weihua Qiu, and Li Liu

J. Biobased Mater. Bioenergy 14, 294–302 (2020)

[\[Abstract\]](#) [\[Full Text - PDF\]](#) [\[Purchase Article\]](#)

REVIEW

Degradation Behaviors of Biodegradable Aliphatic Polyesters and Polycarbonates

Yonghang Xu, Fangya Zhou, Danmin Zhou, Jintang Mo, Huawen Hu, Limiao Lin, Jingshu Wu, Mingguang Yu, Min Zhang, and Hong Chen
J. Biobased Mater. Bioenergy 14, 155–168 (2020)

[\[Abstract\]](#) [\[Full Text - PDF\]](#) [\[Purchase Article\]](#)

RESEARCH ARTICLES

Bubble Wall Rupture Model for Open Cell Structure in Starch/Fiber Heterogeneous Composites

Chuan-Wei Zhang, Fang-Yi Li, Jian-Feng Li, Hai-Yang Lu, and Geng Wang
J. Biobased Mater. Bioenergy 14, 169–177 (2020)

[\[Abstract\]](#) [\[Full Text - PDF\]](#) [\[Purchase Article\]](#)

Production of Phenolic-Rich Bio-Oil from Catalytic Fast Pyrolysis of Biomass Over Tailored Fe-Based Catalysts

Shuangxia Yang, Xiaodong Zhang, Feixia Yang, Baofeng Zhao, Lei Chen, Laizhi Sun, Fanjun Meng, Hongyu Si, and Xiping Xie
J. Biobased Mater. Bioenergy 14, 178–185 (2020)

[\[Abstract\]](#) [\[Full Text - PDF\]](#) [\[Purchase Article\]](#)

Improved Mechanical Properties of Jute Fiber/Polypropylene Composite with Interface Modified by Sodium Lignosulfonate

Qianting Wang, Jianjie Wang, Weikang Liang, Zhixiang Cui, and Junhui Si
J. Biobased Mater. Bioenergy 14, 186–194 (2020)

[\[Abstract\]](#) [\[Full Text - PDF\]](#) [\[Purchase Article\]](#)

Naphthalene and Alkyl Naphthalene from Catalytic Fast Pyrolysis of Biomass Over ZSM-5 Aggregates

Fanjun Meng, Qiaoyan Shang, Dongliang Hua, Lei Chen, Laizhi Sun, Shuangxia Yang, Xiping Xie, Baofeng Zhao, and Xiaodong Zhang
J. Biobased Mater. Bioenergy 14, 195–202 (2020)

[\[Abstract\]](#) [\[Full Text - PDF\]](#) [\[Purchase Article\]](#)

Preparation and Characterization of Cellulose Nanofiber/Zinc Oxide Composite Films

Xiuqiang Zhang, Suxia Ren, Xiaofeng He, Lili Dong, Wei Bai, Tingzhou Lei, and Hong Chen
J. Biobased Mater. Bioenergy 14, 203–208 (2020)

[\[Abstract\]](#) [\[Full Text - PDF\]](#) [\[Purchase Article\]](#)

Improving the Quality of Crop Residues by the Reduction of Ash Content and Inorganic Constituents

Yige Peng and Anthony K. Lau
J. Biobased Mater. Bioenergy 14, 209–219 (2020)

[\[Abstract\]](#) [\[Full Text - PDF\]](#) [\[Purchase Article\]](#)

Catalytic Transfer Hydrogenation of Biomass Derived 5-Hydroxymethylfurfural into 2,5-Dimethylfuran in a Methanol Medium

Kaili Zhang, Danni Li, Ying Liu, and Shubin Wu
J. Biobased Mater. Bioenergy 14, 220–226 (2020)

[\[Abstract\]](#) [\[Full Text - PDF\]](#) [\[Purchase Article\]](#)

Thermal, Biodegradability and Water Barrier Properties of Bio-Nanocomposites Based on Plasticised Sugar Palm Starch and Nanofibrillated Celluloses from Sugar Palm Fibres

R. A. Ilyas^{1,2,3,*}, S. M. Sapuan^{1,2,3,*}, Rushdan Ibrahim⁴, Hairul Abral⁵, M. R. Ishak⁶, E. S. Zainudin^{2,3}, A. Atiqah⁷, M. S. N. Atikah⁸, Edi Syafri⁹, Mochamad Asrofi¹⁰, and R. Jumaidin¹¹

¹Laboratory of Biocomposite Technology, Institute of Tropical Forestry and Forest Products, Universiti Putra Malaysia, 43400, UPM Serdang, Selangor, Malaysia

²Department of Mechanical and Manufacturing Engineering, Universiti Putra Malaysia, 432400 UPM Serdang, Selangor, Malaysia

³Advanced Engineering Materials and Composites Research Centre, Department of Mechanical and Manufacturing Engineering, Universiti Putra Malaysia, 43400, UPM Serdang, Selangor, Malaysia

⁴Pulp and Paper Branch, Forest Research Institute Malaysia, 52109, Kepong, Selangor, Malaysia

⁵Department of Mechanical Engineering, Andalas University, 25163, Padang, Sumatera Barat, Indonesia

⁶Department of Aerospace Engineering, Universiti Putra Malaysia, 43400, UPM Serdang, Selangor, Malaysia

⁷Institute of Power Engineering, Universiti Tenaga Nasional, 43000, Kajang, Selangor, Malaysia

⁸Department of Chemical and Environmental Engineering, Universiti Putra Malaysia, 43400, UPM Serdang, Selangor, Malaysia

⁹Department of Agricultural Technology, Agricultural Polytechnic, Payakumbuh, West Sumatra 26271, Indonesia

¹⁰Laboratory of Material Testing, Department of Mechanical Engineering, University of Jember, Kampus Tegalboto, Jember 68121, East Java, Indonesia

¹¹Fakulti Teknologi Kejuruteraan Mekanikal dan Pembuatan, Universiti Teknikal Malaysia Melaka, Hang Tuah Jaya, 76100, Durian Tunggal, Melaka, Malaysia

Sugar palm (*Arenga pinnata*) starch and fibre are considered as a waste product of the agro-industry. The purpose of the current study is to determine the thermal, water barrier, and soil degradation properties of biodegradable plasticised sugar palm starch (PSPS) that contains sugar palm nanofibrillated celluloses (SP-NFCs) derived from sugar palm fibre. The bio-nanocomposites were fabricated by using the solution-casting method with the nanocellulose contents in the range of 0.1 wt.%–1.0 wt.%. The thermal stability, water resistance and degradation behaviour improved with increase in SP-NFCs content, due to high compatibility and strong inter-molecular hydrogen bonds formed between PSPS and SP-NFCs. PSPS/SP-NFCs bio-nanocomposites with 1.0 wt.% SP-NFCs content displayed the highest mechanical and thermal stability. Residue that was left during the TGA analysis increased as the SP-NFCs content was increased. Soil burial tests showed biodegradability resistance of the bio-nanocomposites. The following conclusions can be drawn from the present reinforcement study of SP-NFCs enhanced biodegradability, water barrier as well as thermal properties of starch polymer which extended the prospective application of environmentally-friendly polymer material. Potential applications for this eco-material are short product life cycles (plastic packaging and food container).

Keywords: Sugar Palm Starch, Nanofibrillated Celluloses, Bio-Nanocomposites, Thermal Properties, Water-Barrier Properties, Soil Degradation.

1. INTRODUCTION

Advanced technology in packaging films derived from petroleum-based product has offered numerous advantages

to humans. Nevertheless, today it is obviously seen that the environmental ecology is extensively distressed and impaired by way of the excessive usage of unbiodegradable petroleum-based products. This has drawn the attention of engineers and material scientists towards renewable, biodegradable and recyclable food packaging

*Authors to whom correspondence should be addressed.

Emails: ahmadilyasrushdan@yahoo.com, sapuan@upm.edu.my

materials [1–4]. Among all biodegradable polymers, such as starch, poly-lactic acid (PLA), polyhydroxyalkanoates (PHAs), polybutylene succinate (PBS), polycaprolactone (PCL), polybutyrate (PBAT), polyvinyl alcohol (PVOH) and polytrimethylene terephthalate (PTT), starch is considered as one of the most attractive and promising materials for biodegradable plastics due its low cost, renewability, abundant supply, availability, ease of chemical modification and biodegradable in nature [5–10].

By incorporating plasticising agent materials, for example, water into starch with the introduction of heat and mechanical energy, through the process of destructureisation, starch can be fabricated into plasticised starch (PS). In the past decade, PS has attracted increasing attention due to its rapid degradation and it also offered substitution for petroleum-based polymer, in which long-term lastingness is not required [11–13]. PS has great commercial prospective for bioplastic. However, according to Sahari et al., [14] and Sanyang et al., [15], PS for packaging application was characterised to have low values in terms of water barrier resistance, heat distortion temperature, easy to dissolve, and low melting viscosity for processing. These problems have limited their wide range of applications, specifically for the application in food packaging [8, 16–18].

Therefore, to overcome the poor water barrier resistance property of PS, many experiments were conducted in engineering and material science [19]. Modification or alteration of the starch polymer via innovative technology is a challenge for scientists who are working on this subject. One of the innovative ways is by reinforcing starch polymers with nanofiller, such as nanocellulose (nanocrystalline cellulose, nanofibrillated cellulose and bacterial nanocellulose), to prepare a bio-nanocomposite. This nano-reinforcement has been verified by various research as an alternative and effective approach to overcome the problems that exist with PS, which are both poor in mechanical and water barrier properties [20–23]. The new generation of bio-nanocomposites can be classified as bio-nanocomposites which comprise the combination of matrix (resin) and natural fibres, usually derived from a plant or cellulose that has at least one dimension scale sized in the range of between 1 nm and 100 nm.

Nanofibrillated celluloses (NFCs) have attracted considerable attention due to their uniqueness and remarkable properties as compared to other commercial fibres (i.e., immense aspect ratio, highly compatible with starch biopolymer, cost effectiveness, featherweight, large surface area to volume ratio with abundance of hydroxyl group on their surface, excellent electrical, mechanical, thermal, as well as biodegradability properties) [24, 25]. In past decades, there were many different agro-wastes used in nanocellulose preparation, such as banana peels [26], rice straw [27], wheat straw [28], soy hull [29], coconut husk [30] mengkuang leaves [31], sugarcane

bagasse [32], and pineapple leaves [33]. Sugar palm is classified as a rapid-growth plant and renewable natural bioresource that can be found growing in South Asia (India, Sri Lanka, Nepal and Bangladesh) to South-east Asia (Malaysia, Burma, Philippines, East Timor, Indonesia, Vietnam, Thailand), and as far as West Africa region (The Gambia) [34–38]. Besides being a multipurpose plant grown in tropical countries, sugar palm tree is also well-known as a prospective source for its starch-biopolymer and natural fibre which can be obtained through its stem and fibre, respectively [16, 39, 40]. Nevertheless, to date there are limited work that were done on the isolation of nanofibrillated celluloses from sugar palm fibres (SPF) and their reinforcement with PS from sugar palm stem itself. Usually, sugar palm starch (SPS) is extracted from sugar palm trees stem that are not capable of producing syrup (*neera sap*) or fruits. Currently in Malaysia, sugar palm trees are planted for their fruits and sap. After these main products are extracted out, the undesired plant components, such as sugar palm fibres and stem, are dumped to decompose naturally [41]. As sugar palm fibres (SPF) are rich in cellulose content, previous research revealed that SPF have great potential as a reinforcing component in many high-performance polymer biocomposite applications [42–44]; hence, increasing their commercial values as byproduct from sugar palm cultivation. Therefore, this present work continues with the isolation of nano-sized sugar palm nanofibrillated cellulose (SP-NFCs) reinforced sugar palm starch biopolymer.

To the best of knowledge, studies on sugar palm nanofibrillated cellulose (SP-NFCs) reinforced sugar palm starch (SPS) biopolymer composites are not found in literature. Therefore, in this work sugar palm nanofibrillated cellulose (SP-NFCs) are isolated from sugar palm fibres (SPF) by using high pressurised homogenisation. After that, to fabricate a high performance bio-nanocomposite, the isolated NFCs with various blend ratios were used to reinforce plasticised sugar palm starch (PSPS)-based polymers in the presence of sorbitol-glycerol plasticiser by using the solution casting method. The effect of nanofibrillated celluloses as nanofillers at different concentrations (0 wt.%, 0.1 wt.%, 0.2 wt.%, 0.3 wt.%, 0.4 wt.%, 0.5 wt.% and 1.0% wt.% dry starch-based) on the soil degradation, water barrier (WVP), and thermal (TGA, DSC and DMA) properties of SP-NFCs/PSPS biofilms were examined.

2. EXPERIMENTAL DETAILS

2.1. Materials and Chemicals

In this work, sugar palm starch (SPS) and sugar palm fibres (SPF) were extracted from sugar palm tree located in Jempol, Negeri Sembilan, Malaysia. The chemical substances used in this experiment were plasticisers (sorbitol and glycerol), acetic acid (CH_3COOH), sodium chlorite (NaClO_2) and sodium hydroxide (NaOH). These chemical

substances were supplied by Sue Evergreen Sdn. Bhd., in Semenyih, Malaysia.

2.2. Sugar Palm Starch Extraction and Preparation

The sugar palm starch (SPS) was obtained from the stem of a matured sugar palm tree. Initially, the tree was cut by using a chainsaw and the mixture of woody fibres and starch powder from the interior part of the stem was collected. Then the mixture was washed prior to filtration to separate the starch from fibres. The fibre remained on top of the sieve, while water carried starch granules in the suspension that was collected in a container after passing through a sieve. Starch which is denser than water settled at the bottom of the container and excess water flowed over the sides. After the process, the fibrous remnants or the by-products were discarded and wet starch was taken out from the container to dry in an open air for 30 min. Finally the starch was oven dried at 120 °C for 24 h [45].

2.3. Sugar Palm Fibre Extraction and Preparation

SPF that was naturally found wrapping the trunk of sugar palm trees from bottom to top was removed by using an axe. This was done prior to grinding and screening in a Fritsch pulverisette mill to convert it into a preferred size of 2 mm [23].

2.4. Cellulose Extraction

Delignification and mercerisation techniques were used in the extraction of cellulose fibres from the SPF [46]. The preparation of holocellulose through a bleaching process, which involved chlorination, was carried out according to the ASTM D1104-56 [47] standard. Then, the ASTM D1103-60 [48] standard was employed on the holocellulose to produce α -cellulose.

2.5. Isolation of Sugar Palm Nanofibrillated Cellulose (SPNFCs)

2.5.1. Mechanical Pre-Treatment

A refining treatment before high pressurised homogenisation (HPH) process was required to enhance fibre accessibility and processing efficiency. Therefore, the sugar palm cellulose (SPC) was refined in 20,000 revolutions in a PFI-mill according to the ISO 5264-2 [49] standard. The process of refining the fibres improved external and internal fibrillations. Moreover, this process also improved the flow of fibres and avoided clogging during fluidisation.

2.5.2. Mechanical High Pressurize Homogenization (HPH)

Nanofibrillated cellulose from sugar palm fibre cellulose was isolated by high pressurised homogenisation (HPH). Typically, 1.8% of fibre suspension was processed in a high pressurised homogeniser (GEA Niro Soavi, Panda NS1001L, Parma, Italy). The samples were passed for

15 times through an intensifier pump that increased the pump pressure, followed by an interaction chamber that defibrillated the fibres by shear forces which had impacts on the channel walls and colliding streams. During this process, fibres were broken down from macro-sized to nano-sized, to form slurries of nanofibrillated cellulose. The high pressurised homogeniser was maintained to operate at 500 bar and under neutral pH value. The temperature was not fixed at a certain value. However, fluidisation was temporarily stopped when the suspension temperature increased to approximately 90 °C. This was to prevent pump cavitation. The process was then continued when the samples had cooled down to approximately 45 °C. Then the NFCs suspensions were collected and freeze-dried at -110 °C by using ethylene gas as the medium and stored in cool place prior to sample analysis [50].

2.6. Preparation of the PSPS/SPNFCs Nanocomposite Films

Plasticiser sugar palm starch/ sugar palm nanofibrillated celluloses (PSPS/SPNFCs) composite films were prepared by using the solution casting method. Initially, SPNFCs and distilled water were mixed and sonicated together to obtain a homogenous nanocomposite film, starch, glycerol and sorbitol. SPNFCs solutions were prepared by mixing and sonicating them with 190 mL of distilled water with different concentrations of SPNFCs (0.1 wt.% to 1.0 wt.% on the starch basis) for 30 min. Then, 10 g of SPS and plasticiser (30% on the starch basis) were mixed with the prepared solutions and stirred in a disperser at 1000 rpm for 20 min at 85 °C for the starch to gelatinise. This step was carried out to ensure that the starch granules had a uniform degradation and a homogeneous dispersion was simultaneously formed. The plasticiser ratio to sorbitol and glycerol combination ratio used was 1:1. Next, the film-forming suspension was allowed to cool down in vacuum condition to get rid of air bubbles present in the suspension prior to the casting of 45 g of the suspension into each petri dish of 15 cm diameter. The dish and its content were put in an oven overnight at a set temperature of 40 °C. The control sample in this study was wholly formed PSPS films that lacked any form of reinforcement (nomenclature as PSPS film). PSPS films were also prepared without SPNFCs that served as the control experiment (designed as PSPS film), while the nanocomposite film with different loading concentrations of 0.1 wt.%, 0.2 wt.%, 0.3 wt.%, 0.4 wt.%, 0.5 wt.% and 1.0 wt.% SPNFCs were denoted as PSPS/SPNFCs-0.1, PSPS/SPNFCs-0.2, PSPS/SPNFCs-0.3, PSPS/SPNFCs-0.4, PSPS/SPNFCs-0.5 and PSPS/SPNFCs-1.0, respectively. Prior to any characterisation analysis, the ensuing films were stored for 7 days in the desiccator (23 ± 2 °C and 53 ± 1% RH) to guarantee consistency of water contained in the stored films.

2.7. Characterisation

2.7.1. Thermal-Gravimetric Analysis

The thermal degradation behaviour of bio-nanocomposites was evaluated by thermo-gravimetric analysis with respect to weight loss due to increase in temperature. To define the bio-nanocomposite thermal stability, TGA analysis was executed with a Q series thermal analysis machine from TA Instruments (New Castle, DE, USA). The analysis was carried out under a dynamic nitrogen atmosphere in temperature range of 25 °C–800 °C at a heating rate of 10 °C min⁻¹, in which 10 mg was placed in aluminum pans. TGA curve of percentage weight loss against temperature gained from the TGA analysis was used to determine the weight loss of the bio-nanocomposite films [51].

2.7.2. Differential Scanning Calorimeter

A DSC characterisation was also performed on the samples. In this case, the samples were heated in a temperature range of 35 °C–200 °C at a 10 °C min⁻¹ heating rate. 10 mm² of each film sample was subjected to the conditioning parameters of 60% RH and 25 °C temperature. The following factors were gained by these thermo-grams: the onset temperature (T_o) and the peak temperature (T_p).

2.7.3. Dynamic Mechanical Analysis (DMA)

The dynamic mechanical analysis (DMA) for various bio-nanocomposite films were analysed by using the ASTM D5026 [52] standard method. The estimations were done by utilising a dynamic mechanical analyser in the operating condition of 1 Hz frequency in tension mode and 0.01 N pre-loading forces. In an attempt to properly place the sample on the specimen holder which contained the film tension apparatus, the sizes of bio-nanocomposite films were accustomed to 0.2 nm–0.5 mm, 10 mm and 30 mm, which represented its thickness, wide and length, respectively. The analyses of dynamic storage modulus and loss modulus were carried out under the optimal operating conditions of 25 °C–150 °C temperature range and 2 °C/min steady heating rate.

2.7.4. Water Vapour Permeability (WVP)

The ASTM E96-95 [53] standard method was used to determine water vapour permeability. The WVP test was repeated 6 times and conducted under a controlled room with temperature and relative humidity (RH) of 23 ± 2 °C and 53 ± 1%, respectively. Twenty gram of silica gel was placed within the container cup, in which the mouth of the container cup was 30 mm in length. Then bio-nanocomposite films were accustomed into round shape and affixed to the mouth of the cylindrical container cups, leaving a 3 mm vacuum to the top of the container cup. The weight of the container cup was weighed and recorded, before the container cup was placed inside a steady relative humidity chamber with temperature

and relative humidity (RH) of 25 °C and 75%, respectively. Container cup weight gain was taken intermittently until the weight of the container approached an equilibrium reading. The water vapour permeability of the bio-nanocomposite film was determined by using the Eq. (1),

$$WVP = \frac{(m \times d)}{(A \times t \times P)} \quad (1)$$

Where, the water vapour permeability is WVP , weight gain by the container test cup is m (g), the thickness of film is d (mm), the exposed surface area of the film is A (m²), the permeation time interval is t (s), and the partial pressure of water vapour over the film sample is P (Pa). The derived unit of the overall outcome is g · s⁻¹ · m⁻² · Pa⁻¹.

2.7.5. Biodegradability Test

According to the technique depicted by Edhirej et al. [54], biodegradability test was conducted by assessing the reduction weight of the bio-nanocomposites with size of 30 mm by 20 mm buried in 100 mm depth in characterised soil. The soil physico-chemical properties were determined, potassium: 45.93 μg/g; total nitrogen: 0.07%; phosphorus 96.6 μg/g; organic carbon: 1.14%; and pH: 6.52. The biodegradability test was repeated 3 times and conducted under moisture controlled condition. The soil was frequently moisturised by distilled water. Each sample was taken from the soil by following a periodic burial time interval of 24 h, 48 h, 72 h, 168 h, 216 h and 264 h. After that, the samples were carefully washed and dried by using vacuum oven that was set at 60 °C. The samples were then placed into the desiccators to gain a constant weight. The reduction weight of the films was then determined by utilising Eq. (2), in which weight before being buried = W_0 , weight after being buried = W_t .

$$\text{Weight loss (\%)} = \frac{W_0 - W_t}{W_0} \times 100 \quad (2)$$

2.7.6. Statistical Analysis

PSPS statistical analysis software was conducted to perform the analysis of variance (ANOVA) on the obtained experimental results. To conduct the mean comparisons at 0.05 levels of significance ($p \leq 0.05$), a test known as Tukey test was used.

3. RESULTS AND DISCUSSION

3.1. Thermal Analysis

Figure 1 shows the TG curve (DTG and TGA curves) of the control PSPS film and PSPS/SPNCCs bio-nanocomposite films, in which these curves represent the thermal stability and thermal degradation of the films. From Figure 1, it can be seen that the TG curves of the starch based-film of PSPS film and PSPS/SP-NFCs films formed a multi-step thermal degradation, in which these outcomes with two thermal degradations were also well

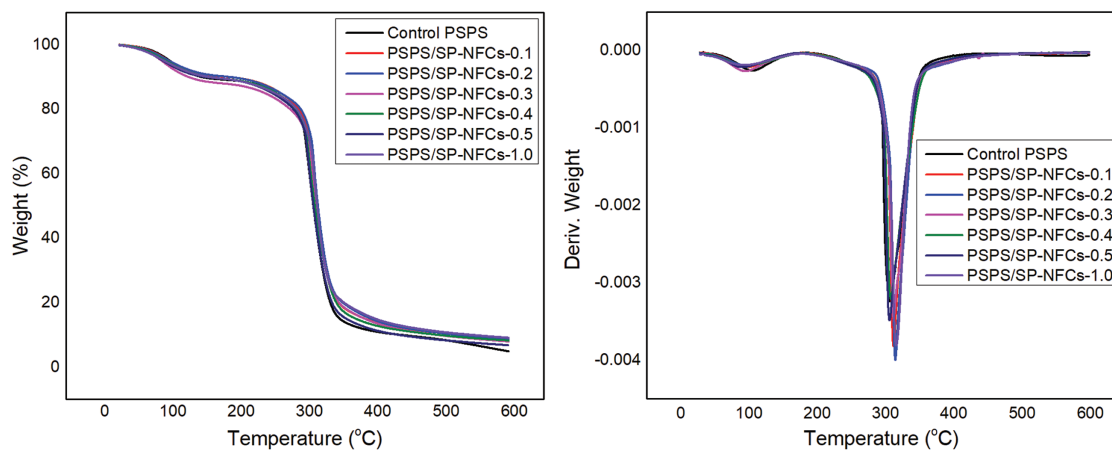


Fig. 1. TG curves (DTG and TGA) of control PSPS film and PSPS/SP-NFCs bio-nanocomposite films with various concentrations.

reported and supported by other works reported in the literature [55].

The first degradation step occurred below 100 °C, which was approximately at 40 °C to 47 °C and this was due to the elimination of film's water content. Moreover, the mass of biofilm loses at this phase could be attributed to the dehydration of loosely bound water and evaporation of low molecular weight compounds within the control and bio-nanocomposite films [2].

The DTG curve of control PSPS film showed a crest peak at 305.14 °C with 79.13% of the weight of the film loss, as the sample was further heating. This phenomenon might be attributed to the decomposition of saccharide rings of the control PSPS film [5]. Besides, control film PSPS displayed a huge mass loss in comparison to the PSPS/SP-NFCs bio-nanocomposite films within temperature lower than 100 °C. However, the PSPS/SP-NFCs bio-nanocomposite films showed lower mass loss in comparison to control PSPS film, which was attributed to the higher moisture content of control PSPS film as compared to PSPS/ SP-NFCs bio-nanocomposite films.

The evaporation of chemisorbed water molecules and glycerol plasticised compound occurred in the second phase of the thermal decomposition in the range of ~125 °C–290 °C. The results of the decomposition temperatures of PSPS/SP-NFCs bio-nanocomposite films

and control glycerol-plasticised PSPS corroborated with the findings of previous work in plasticised sugar palm starches by Sahari et al. [56] and Sanyang et al. [55]. Moreover, there were similarities between the properties expressed by Zhong et al. [57], where the study found that the thermal decomposition of glycerol plasticised compound of kudzu starch-based films was in the range of 150 °C–280 °C.

Besides, a severe weight reduction and a higher thermal decomposition rate of control PSPS film and PSPS/SP-NFCs bio-nanocomposite films were observed when the films were further heated beyond 290 °C. The onset of thermal degradation of both control PSPS and PSPS/SP-NFCs bio-nanocomposite films took place at temperature of around 300 °C. This was due to the degradation and depolymerisation of starch carbon chain polymers as well as elimination of hydrogen groups within the plasticised starch-based [58, 59].

From the thermal degradation curve, T_{max} of films data in Table I, it is apparent that the PSPS/SP-NFCs bio-nanocomposite films had greater thermal stability values as compared to control plasticised PSPS which were 305.14 °C and 316.92 °C, respectively. There are several possible explanations for these results: incorporation of nanocellulose within the PSPS resulted in formation of hydrogen-bonding interactions between SP-NFCs

Table I. Transition glass temperature (T_g), onset temperature (T_{onset}), temperature of the maximum weight-loss rate (T_{max}), weight loss (W_L) and yield of char for control PSPS film and PSPS/SP-NFCs bio-nanocomposite films with various SP-NFCs content gained from the analysis of DSC, DTG and TG curves.

Sample	T_g		Water evaporation		1st thermal degradation			Char yield
	$T_{g, mid}$ (°C)	T_{onset} (°C)	T_{Max} (°C)	W_L (%)	T_{onset} (°C)	T_{Max} (°C)	W_L (%)	W (%)
Control PSPS	37.91	40.24	104.07	10.54	187.11	305.14	79.13	4.91
PSPS/SP-NFCs-0.1	42.66	29.42	94.82	10.38	177.83	305.6	78.29	8.26
PSPS/SP-NFCs-0.2	42.9	31.16	93.92	10.13	183.25	308.17	76.56	6.84
PSPS/SP-NFCs-0.3	31.4	31.4	87.8	10.81	187	309.12	77.78	7.53
PSPS/SP-NFCs-0.4	37.91	31.71	98.4	9.65	179.37	309.49	78.62	8.44
PSPS/SP-NFCs-0.5	39.01	30.55	96.81	9.52	176.66	312.24	79.09	8.63
PSPS/SP-NFCs-1.0	49.15	27.49	95.09	10.24	184.26	315.81	77.13	9.12

nanofiller and starch-based matrix. These bondings contributed to a restriction of matrix chain mobility, which indirectly improved the PSPS/SP-NFCs polymer thermal stability. These results were in agreement with previous studies for incorporation of nanocellulose into polyvinyl alcohol (PVA) [60] and starch [61]. The higher the concentration of SP-NFCs, the stronger was the bonding between the polymers. This outcome was consistent with the weight loss reduction of bio-nanocomposite films at temperature of >300 °C, in which the higher the SP-NFCs loading, the lower the weight loss.

Char can be classified as solid substances or materials that are leftovers after all volatile components in the substance are released or driven out from a carbonaceous material during the combustion stage, which is known as pyrolysis, carbonisation, devolatilisation or charring. In addition, it can be observed that the char leftover yield of biofilms showed an increased char residue (4.91%–9.12%) with the increment of the 1.0 wt.% SP-NFCs content in the PSPS as compared to control PSPS. Several possible explanations for these results: (1) nano-sized scale fibril and huge number of free-end chains of SP-SPNFCs, in which the end-chains of SP-NFCs decomposed at low temperature [62], and (2) lower water content of PSPS/SP-NFCs bio-nanocomposite films, as compared to control PSPS at equilibrium state. As the SP-NFCs was highly crystalline structure (81.19%) [25], its structure crystallinity reduced the polar character of starch. Therefore, the increasing content incorporation of SP-NFCs within the PSPS, would reduce the water content which resulted in low char leftover [20].

3.2. Differential Scanning Calorimeter (DSC)

The structure and interaction between nanofiller and matrix analysis was performed via DSC analysis for temperature range of 25 °C–200 °C. The glass transition temperature (T_g) is denoted as inflection point of specific heat increment under the glass-rubber transition. The values of T_g for all nanocomposites are as tabulated in Table I. Strong interactions were observed among the SP-NFCs nanofiller molecules and among the nanofiller molecules and the PSPS biopolymer matrix molecules that were present with the addition of the nanocellulose; meanwhile the interactions between PSPS molecules had been eliminated. From Figure 2(d) it was obvious that all film samples showed only one distinct heat increment, which corresponded to the glass transitions of sugar palm starch-based matrix. No endothermic peak, assigned to the melting of water-induced crystalline amylopectin domains, was observed in the temperature region of 100 °C–200 °C, which indicated the amorphous nature of PSPS matrix. The PSPS matrix displayed the T_g transition at about 37.91 °C.

According to Dufrense et al., [63], the PSPS plasticised by glycerol existed as a complex heterogeneous system, consisting of glycerol-rich domains dispersed in a starch-rich continuous phase, whereby each phase should have

exhibited its own T_g . Therefore, these transitions occurred in the temperature range from -80 °C– 50 °C and from 30 °C– 60 °C which were associated with the glass transitions of the glycerol-rich phase and starch-rich phase, respectively. Nevertheless, the T_g transition of glycerol-rich phase located in the temperature region from -80 °C– 50 °C, could not be determined due to the limitation of refrigerated cooling systems of DSC. Besides, with the increasing SP-NFCs nanofiller from 0 wt.%–1.0 wt.%, there was obvious change in value of T_g for starch-rich phase that shifted to a higher temperature from 37.91 °C–49.15 °C. The increase in T_g dependence on the concentration of SP-NFCs might be attributed to the occurrence of intermolecular interactions between stiff SP-NFCs and PSPS matrix, which restricted the mobility and flexibility of the amorphous starch chains in contact with the high surface area of SP-NFCs [23]. The increasing trend of the T_g , which was also well-defined as the mid-point temperature of glass transition, from 37.91 °C–49.15 °C might be attributed to the strong interaction between the PSPS molecules instantly destroyed by the addition of SP-NFCs nanofiller, leading to an enhancement of PSPS molecular mobility.

3.3. Dynamic Mechanical Analysis (DMA)

One of the parameters studied from DMA testing was loss factor. It can be described as the recoverable strain energy in the distorted samples related to material molecular motion. This term is defined as the ratio of loss modulus to storage modulus ($\tan \delta = E''/E'$). The glass transition temperature (T_g) is represented with $\tan \delta$ values of the film samples [5]. Figure 2 represents the variation of (a) storage modulus (E'), (b) loss factor ($\tan \delta$), (c) loss modulus (E''), and differential scanning calorimetry (DSC) of PSPS and PSPS/SP-NFCs bio-nanocomposites films as a function of temperature. The DMA curves of PSPS and PSPS/SP-NFCs films and their individual components showed similar trends in the discrepancy of E' and E'' with temperature. Figure 2(b) also shows that the loss factor ($\tan \delta$) curves for all film samples increased gradually until they reached the peak values.

From Figure 2(a), it was proven that an increase in the amount of SP-NFCs nanofibre from 0.1%–1.0% had increased the storage modulus of the films. The current study showed that storage modulus (E') for control film was approximately 51.41 MPa at 25 °C, while that in PSPS/SP-NFCs-1.0 was about 1103.07 MPa. The storage modulus of bio-nanocomposite films had increased by 2045% as compared to the control films. Besides, the reduction of the bio-nanocomposite films modulus, as a result of increase in temperature, was found to be more significant for films at low concentrations of SP-NFCs nanofiller. This finding verified that at high temperatures, a significant amount of load was borne by the physically entangled network of nanofibres in the bio-nanocomposites [54]. This also showed that the capacity

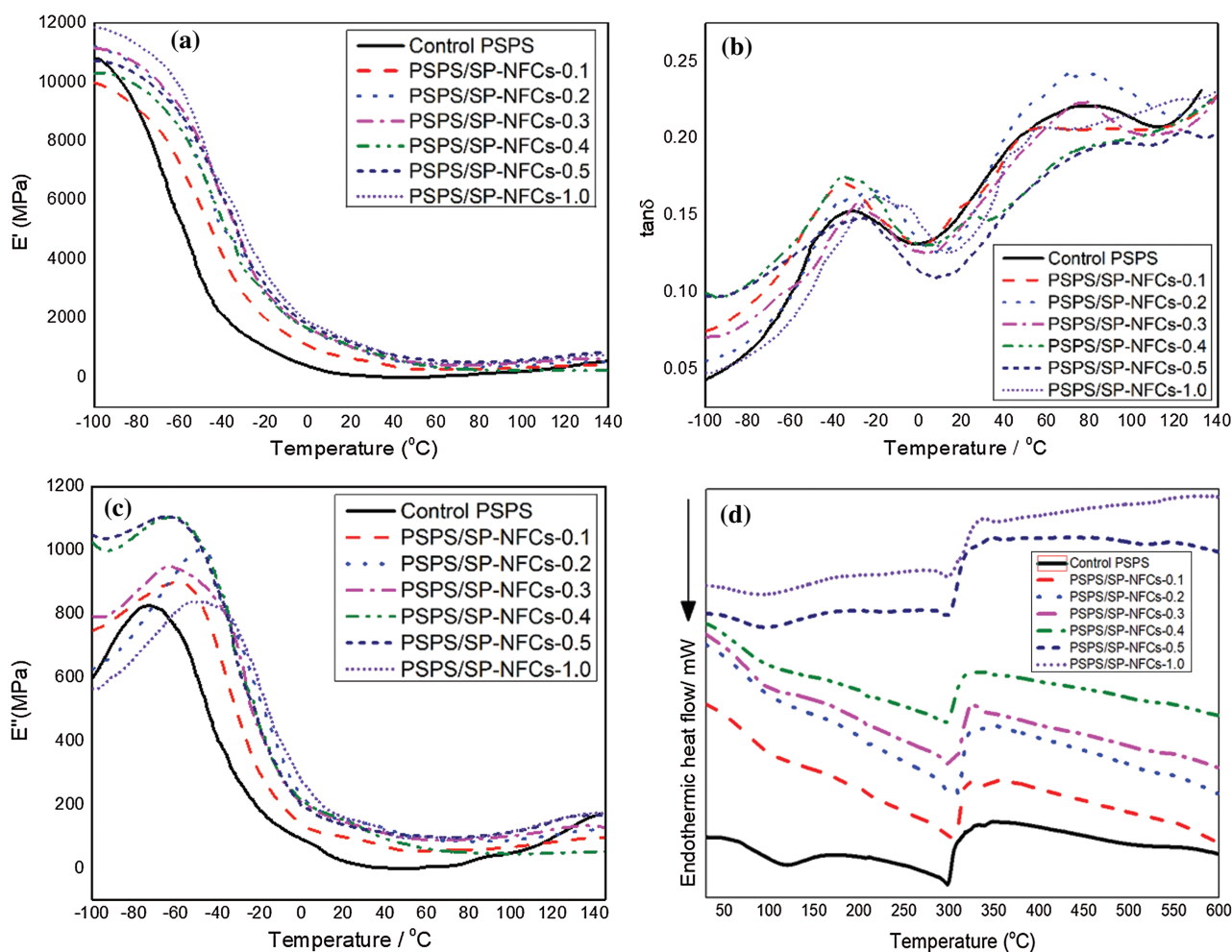


Fig. 2. DMA analysis: (a) Storage modulus (E'), (b) loss modulus (E''), (c) loss factor ($\tan \delta$); and DSC analysis: (d) differential scanning calorimetry thermograms of control PPS and PPS/SP-NFCs bio-nanocomposite films as a function of temperature.

of the matrix to reduce mechanical restrictions with recoverable viscoelastic distortion was increased by SP-NFCs nanofiller. The higher E' values were observed from the bio-nanocomposite films as compared to the matrix (control film) and displayed certain tendencies with respect to the concentration of SP-NFCs nanofiller. This beneficial tendency might be attributed to the quill nanofibres that have high compatibility with the polymer matrix, leading to good dispersion and large area of interface. Conversely, excess reinforcement had caused slight decrease in the film bio-nanocomposite with higher concentration, which was probably due to insufficient capability of the matrix to completely cover and wet the quill nanofibres. This outcome was also supported by Savadekar and Mhaske [64].

Besides, their corresponding T_g transitions are displayed in Figure 2(b) as a function of nanofiller SP-NFCs contents. The maximum $\tan \delta$ peak resembled the glass transition, in which DMA measured the change in mechanical response of these polymer chains. In Figure 2(a), a two-step decrease of the storage modulus (E') at the temperature from -70 °C to -40 °C and from 20 °C to

-60 °C, are observed, respectively, which were attributed to the T_g transition of glycerol-rich phase and starch-rich phase, observed for all films. The bio-nanocomposite films which contained of 0.1 wt.% SP-NFCs and above behaved as rubber due to their storage modulus values were nearly constant over a broad temperature range above T_g , and displayed a greater increase in E' with increasing SP-NFCs concentrations. For example, the storage modulus (E') of PPS/SP-NFCs-1.0 was about 21.5 and 2.6 times higher than that of PPS films at the 25 °C and 100 °C, respectively. It was an indication of reinforced rigidity and enhanced thermal stability of the starch-based bio-nanocomposite films, which can be attributed to the strong interfacial interactions between large specific SP-NFCs surface area and starch matrix. Furthermore, it was also showed that the matrix capacity to reduce mechanical limits with recoverable viscoelastic deformation was improved by SP-NFCs nanofiller.

The changes of the loss modulus (E'') versus temperature curve for control PPS film and PPS/SP-NFCs bio-nanocomposite films are displayed in Figure 2(c),

whereby all E'' curves displayed wide peaks (from 50 °C–100 °C) with separate positions of amplitude and temperature. This phenomenon was associated to the “ α ” peaks and suggested more complex structural relaxation behaviour in the bio-nanocomposites. This phenomenon of structural relaxation might be attributed to the movement of starch polymeric matrix chain, whereby at room temperature, all bio-nanocomposite peaks were moved to higher temperatures as compared to PSPS film. These occurrences might be attributed to the reduction in the movement of the polymer chains initiated by the addition of SP-NFCs nanofibres. In addition, for polymer composites, a significant decrease in chain flexibility happened when the peaks of E'' were shifted to higher temperatures. Besides, it can be observed from Figure 2(c) that as higher concentration of SP-NFCs nanofibres was reinforced, the increment rate of E'' flow became lowered and the E' became higher as a function of temperature. Theoretically, the viscosity of the polymer matrix gradually decreases when the temperature increases. Wide peaks were seen along the curves within the temperature range of 40 °C–70 °C, which indicated the transitional region from glassy to rubber state. The rise denoted that loss modulus (E'') decreased with temperature slower than E' did. Similar finding was also found in the study of incorporation of orange albedo nanocellulose and high amylose starch [65].

The $\tan \delta$ -T curves of control PPS and PPS/SP-NFCs bio-nanocomposite films were gradually increased until peak values were obtained. The $\tan \delta$ peaks of the bio-nanocomposite matrix moved to higher temperatures when the concentration of SP-NFCs nanofiller increased. As the nanofiller contents were increased from 0 wt.%–1.0 wt.%, the shifts of relaxation peaks move from –30.5 °C–18.6 °C were observed. The relaxation peak of PPS at higher temperature shifted from 55 °C–90 °C and became flat, denoting that SP-NFCs restricted the molecular movement of starch due to strong interactions between nanofillers and starch. The mobility of PPS molecules was constrained by the dense concentration and compact arrangement with less free volume of SP-NFCs nanofiller, hence, creating less elastic PPS/SP-NFCs bio-nanocomposite films with the addition of SP-NFCs nanofiller at different concentrations. These results seemed to be consistent with the analysis results obtained from DSC experiment.

Besides, according to Balakrishnan et al. [66], by using storage modulus values, the differential parameters can be predicted, such as degree of entanglement, effectiveness of dispersion and reinforcing efficiency. The effectiveness of SP-NFCs nanofiller incorporated within PPS bio-nanocomposite films can be analysed by using the Eq. (3),

$$E_f = \frac{E'_g/E'_r \text{ Nanocomposites}}{E'_g/E'_r \text{ Matrix}} \quad (3)$$

Where, E_r and E'_g are the indication of storage modulus at rubbery (0 °C) and glassy (–90 °C) phases, respectively,

of the control and bio-nanocomposite films. E_f indicates the effectiveness of dispersion.

The results obtained from the preliminary analysis of E_f of bio-nanocomposite films with different concentrations (wt.%) of SP-NFCs are presented in Table II. The differential parameters of E_f are relative measures of reduction in storage modulus of bio-nanocomposite films as a function of temperature. The observed correlation between effectiveness of the SP-NFCs within starch-base polymer and E_f might be explained in this way: the effectiveness of the SP-NFCs dispersion in PPS is higher when the value of E_f is lower.

It can be seen from Table II that the value of E_f decreased as the concentration of SP-NFCs wt.% increased. However, as the concentration of the SP-NFCs reached 1.0 wt.%, the E_f of the bio-nanocomposite film exhibited insignificant increment. There were several possible explanations for these results: (1) low effectiveness of dispersion of SP-NFCs incorporated PPS during fabrication; (2) low coverage ability of PPS to cover and bind with SP-NFCs completely; (3) accumulation/agglomeration of SP-NFCs at higher concentration wt.% loading; (4) uneven distribution of SP-NFCs in starch-based matrix, which failed to act as reinforcement agent in PPS [2]. Moreover, to obtain a high degree of SP-NFCs reinforcement in PPS film, the entangled monocrytals network that immobilised the starch polymer chain must be high. Some of the E_f issues emerging from these findings related specifically to degree of entanglement (ϕ). Therefore, the ϕ of SP-NFCs inside the PPS-starch based polymer was a crucial aspect that needed to be comprehended due to the good correlation between E_f , in which they correlated to the fine dispersion of SP-NFCs within the surface of PPS bio-matrix.

The degree of entanglement (Φ) of control PPS and SP-NFCs bionanocomposite films were estimated by using the Eq. (4) [67].

$$\Phi = \frac{E'}{6RT} \quad (4)$$

Where T , R , and E' are the indication of temperature in Kelvin, universal gas constant (8.314 kJ mol⁻¹ K⁻¹), and storage modulus at rubbery region (0 °C), respectively.

The results of the correlation analysis of entanglement degree (Φ) of SP-NFCs at different concentrations (wt.%) reinforced PPS bio-nanocomposite films are shown in Table II. From this data, we can observe that the increment of the SP-NFCs concentrations within the PPS bio-matrix resulted in higher value of Φ . It seemed possible that these results were due to the homogeneous dispersion of SP-NFCs within the PPS matrix [66].

The reinforcing ability of SP-NFCs inside PPS was measured by Einstein equation as stated in Eq. (5). [68].

$$E_m(1 + rV_f) = E_c \quad (5)$$

which can be simplified as,

$$r = [(E_c/E_m) - 1]/V_f$$

Table II. DMA data (effectiveness of dispersion, degree of entanglement and reinforcing efficiency) and water vapor permeability (WVP) of PSPS and PSPS/SP-NFCs bio-nanocomposite films in different concentrations.

Wt.% of SP-NFCs	Effectiveness of dispersion (E_f)	Degree of entanglement (ϕ)	Reinforcing efficiency (r)	WVP ($10^{-10} \text{ g} \cdot \text{s}^{-1} \cdot \text{m}^{-1} \cdot \text{Pa}^{-1}$)
0	–	–	–	9.58 ± 0.01^g
0.1	0.336	0.078	4.291	8.07 ± 0.01^f
0.2	0.255	0.116	7.567	7.54 ± 0.08^e
0.3	0.250	0.119	7.823	5.70 ± 0.01^d
0.4	0.233	0.119	7.816	4.04 ± 0.02^c
0.5	0.222	0.129	8.651	2.38 ± 0.05^b
1	0.229	0.137	9.415	1.21 ± 0.02^a

Note *Values with different letters in the same column are significantly different ($p < 0.05$).

Where, r , V_f , E_m and E_c are the reinforcing efficiency of nanofiller to matrix, volume fraction of the filler (obtained by density equation) [69], storage modulus of matrix and bio-nanocomposites at rubbery region (0°C), respectively. Table II presents the results obtained from the differential parameter analysis of reinforcing efficiency of SP-NFCs concentrations (wt.%) within the PSPS matrix.

Besides, it can be observed from the values calculated in Table II that the efficiency of SP-NFCs reinforcement increased with the increment of the concentration up to 1.0 wt.% of SP-NFCs. From the data gained, there was no sign of reinforcing efficiency (r) value that was observed to be reduced.

From Figure 2(d), the addition of SP-NFCs has directed the increase in melting temperature (T_m) and glass transition temperature (T_g). The effect of SPNFC contents on T_g and T_m was obviously seen and an increase in the SP-NFCs level from 0%–1.0% led to the increase in T_g (from 37.91°C – 49.15°C) and T_m (from 297.17°C – 302.00°C). This phenomenon might be due to the existence of restrained chains on the surface of nanofibrillated celluloses. Increasing T_m displayed faster crystallisation induced by SP-NFCs, which acted as nucleating agents for PSPS matrix system. SP-NFCs allowed heterogeneous nucleation mechanism which induced a decrease of the free energy barrier and fastened the crystallisation. This study supported the evidence from previous observations by George et al., [70] and Noshirvani et al., [71] who claimed that this was due to the similarity of chemical structure between PSPS matrix and SP-NFCs nanofiller, that were highly miscible, and hence led to strong hydrogen bond formation between them and restriction of the mobility of polymer chains. Therefore, increment in T_g could occur in the PSPS/SP-NFCs bio-nanocomposite films.

3.4. Water Vapour Permeability

The WVP rate was analysed for control PSPS film and PSPS/SP-NFCs bio-nanocomposite films, and is displayed in Figure 3 and Table II. The WVP of biofilms was reduced with the introduction of SP-NFCs nano-reinforcements. This might be attributed to a water vapour barrier enhancement for the bio-nanocomposite films,

because of the water vapour gas molecules experienced difficulty to penetrate the crystalline region of the cellulose crystals [17]. Besides, the highest WVP value recorded was PSPS film ($9.58 \times 10^{-10} \text{ g} \cdot \text{s}^{-1} \cdot \text{m}^{-1} \cdot \text{Pa}^{-1}$). The PSPS films were swollen, as moisture content was increased, which increased the plasticisation physical properties. As a result, diffusivity also increased significantly. Another possible explanation for this phenomenon was due to their properties of highly hydrophilic in nature and besides, their moisture content sensitivity and surrounding relative humidity factors were difficult to control [72]. Moreover, PSPS films have high tendency to gain changes in both mechanical and physical properties, when the biofilms were exposed during storage time in certain environmental conditions. Physical changes in the properties of the PSPS might be due to the retrogradation (polymer recrystallisation) caused by the migration of low molecular weight constituents, such as water and plasticisers contained in film formulation.

The nano-reinforcements of SP-NFCs within starch significantly increased the WVP of the PSPS bio-nanocomposite films. The incorporation of 0.1% SP-NFCs into control PSPS films decreased their WVP value by

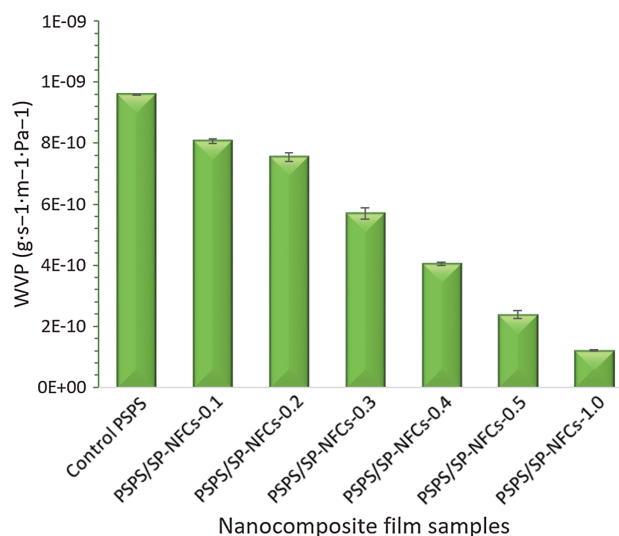


Fig. 3. Effect of SP-NFCs contents (wt.%) on the WVP of the PSPS bio-nanocomposite films, as a function of SP-NFCs content in dry matrix.

15.76%. This reduced value might be attributed to the formation of the highly tortuous diffusion path caused by the presence of rigid crystalline structure and the high distribution of SP-NFCs in the PPS, which prolonged, retarded or hindered the path of water molecules through the film matrix [73]. The uniform dispersion of SP-NFCs forced water vapour molecules to traverse a maze or tortuous path to pass through the bio-nanocomposite film, and thus retarded gas transmission. Increasing the SP-NFCs concentration from 0.1%–1.0% had caused a slight reduction in the WVP of composite films from $8.07 \times 10^{-10} \times \text{g} \cdot \text{s}^{-1} \cdot \text{m}^{-1} \cdot \text{Pa}^{-1}$ – $1.21 \times 10^{-10} \times \text{g} \cdot \text{s}^{-1} \cdot \text{m}^{-1} \cdot \text{Pa}^{-1}$. PPS/SP-NFCs bio-nanocomposite films revealed 87.36% improvement in WVP as compared to control PPS films. Basically, WVP through a hydrophilic film depends on the solubility and diffusivity of water molecules in the film matrix. Therefore, when the bio-nanocomposite structure is formed in a well-dispersed state individual SP-NFCs that has high aspect ratio which is believed to enhance the water barrier property by forming a tortuous or maze path for water molecules to traverse the film matrix. Therefore, this enhances the effective path length for diffusion and retards the progress of water vapour molecules absorption and film diffusivity through the polymer matrix. Besides, the reduction in OH groups, due to the formation of hydrogen-bonding interactions between SP-NFCs nanofiller and starch matrix contributes to a restriction of matrix chain mobility, which indirectly reduces the solubility of water molecules in the matrix [71, 74]. This study was supported by Noshirvani et al., [71], who used cotton linter nanocellulose to reinforce potato starch.

To better understand the mechanisms of water permeability and its effects on PS, Masclaux et al., [75] analysed that the properties of starch nanocomposite films were strongly affected by relative humidity, in which the WVP rate displayed higher in starch films at high relative humidity. High water sorption and diffusion in PPS film might be attributed to the high chain mobility and high swelling capacity. Therefore the addition of nanocellulose to PPS films can improve the water barrier properties of the films.

3.5. Soil Burial Testing

Research on biodegradation properties of bio-nanocomposite films is important for the application as food packaging in environment. Biodegradation is the decomposition of organic materials by the action of bacteria, microorganism and fungi or by other biological means. Initially, the biodegradation of PS starts when these biological microbial organisms interact with the PS films [54]. These biological microbial organisms change the polymer matrix through metabolic or enzymatic process that break down the high average molecular weight polymers matrix into smaller and lower average molecular weight compound can have. As a result, this process leads to the decomposition of material in the

environment and the completed biodegradation process is called mineralisation [76]. In the present experiment, the bio-nanocomposite, incorporating of 0.1 wt.%–1.0 wt.% SP-NFCs nanofibres, as well as the control PPS starch were submitted to biodegradation by soil burial test in perforated polybags. Figure 4 displays the weight loss of the control PPS and PPS/ SP-NFCs bio-nanocomposites as a function of soil burial time. It was noted that weight loss showed gradual increment for the first day and started to slow down for the consequent days with degradation time for both PPS and PPS/SP-NFCs bio-nanocomposite films. After 9 days of soil burial, the weight of control PPS film had lost 85.76%, however the PPS/SP-NFCs bio-nanocomposite films had lost lesser weight as compared to control PPS, which were 75.69%, 74.42%, 73.12%, 72.02%, 69.88% and 68.03% weight for PPS/SP-NFCs-0.1, PPS/SP-NFCs-0.2, PPS/SP-NFCs-0.3, PPS/SP-NFCs-0.4, PPS/SP-NFCs-0.5, and PPS/SP-NFCs-1.0, respectively. It can also be analysed from Figure 4 that the average soil decomposition rate was 7.56%/day and 9.53%/day, respectively, for the PPS/SP-NFCs-1.0 and control PPS films. The weight loss of PPS/SP-NFCs bionanocomposite films was lower than that of the control PPS film at any given time points. After 10 days of soil degradation test, the control PPS film was totally degraded. In the meantime, it took 14 days for PPS/SP-NFCs bio-nanocomposite films to completely decompose. A possible explanation for these results may be: (1) water absorption by film; and (2) degree of crystallinity of SP-NFCs in bio-nanocomposite films [2].

As compared to the PPS/ SP-NFCs bio-nanocomposite films, the weight loss for the control PPS film was higher for all the successive degradation tests. It seemed possible that these results were due to the physical properties of PPS, where PPS absorbed more water as compared to PPS/ SP-NFCs bio-nanocomposite films, making it more visible to biological microbial organism attack [56]. According to Kiatkamjornwong et al., [77], these biological microbial organisms attacked the PPS biodegradable films in the presence of a water medium.

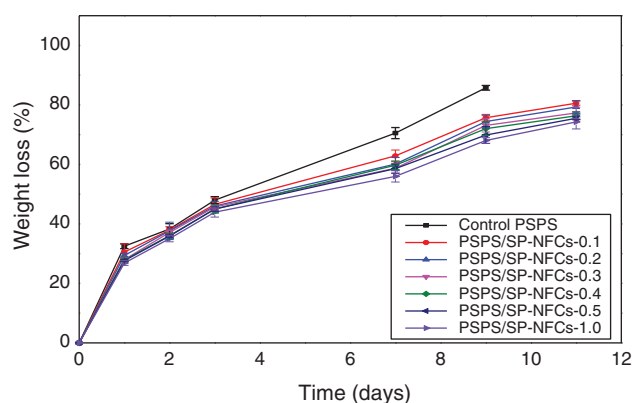


Fig. 4. Weight loss of PPS and PPS/SP-NFCs composite films as a function of soil burial time.

Besides, it is difficult for the biological microorganisms to decompose cellulose due to the physical-chemical properties of the cellulose which are high degree of crystallinity and high degree of polymerisation [78, 79], in which the degree of crystallinity of cellulose is the main structure of SP-NFCs bio-nanocomposite films [80]. These results corroborated with the findings of any previous work in that crystalline regions are difficult to decompose [2, 23, 79, 81]. PSPS/SP-NFCs biodegradable films had higher crystallinity index compared to control PSPS starch-based film, which made them to have a higher resistance to be attacked by microbial organisms as compared to control PSPS film. This caused the difference in weight loss and interfacial strength between control PSPS and the PSPS/ SP-NFCs bio-nanocomposite films. In addition, the variation of resistance to microbial organism

attack between control starch PSPS and PSPS/SP-NFCs showed that in PSPS/SP-NFCs bio-nanocomposite, microbial organism attack started with starch. From the result analysed, SP-NFCs had the minor role, as can be concluded from the slight difference in weight loss suffered by the PSPS and the PSPS/SP-NFCs matrix films in Figure 4. The amorphous region favoured the microbial organisms' accessibility to the matrix films (mainly to the deterioration of starch). When the microorganisms consumed the surrounding PS, the bio-nanocomposite film lost their physical structural integrity, leading to the weakening of the interfacial strength between starch matrix and SP-NFCs, and thus allowing the attack of SP-NFCs by microbial organisms [82]. The study was successful as it could identify the biodegradability behaviours of PSPS/SP-NFCs starch-based bionanocomposite films, in which these films

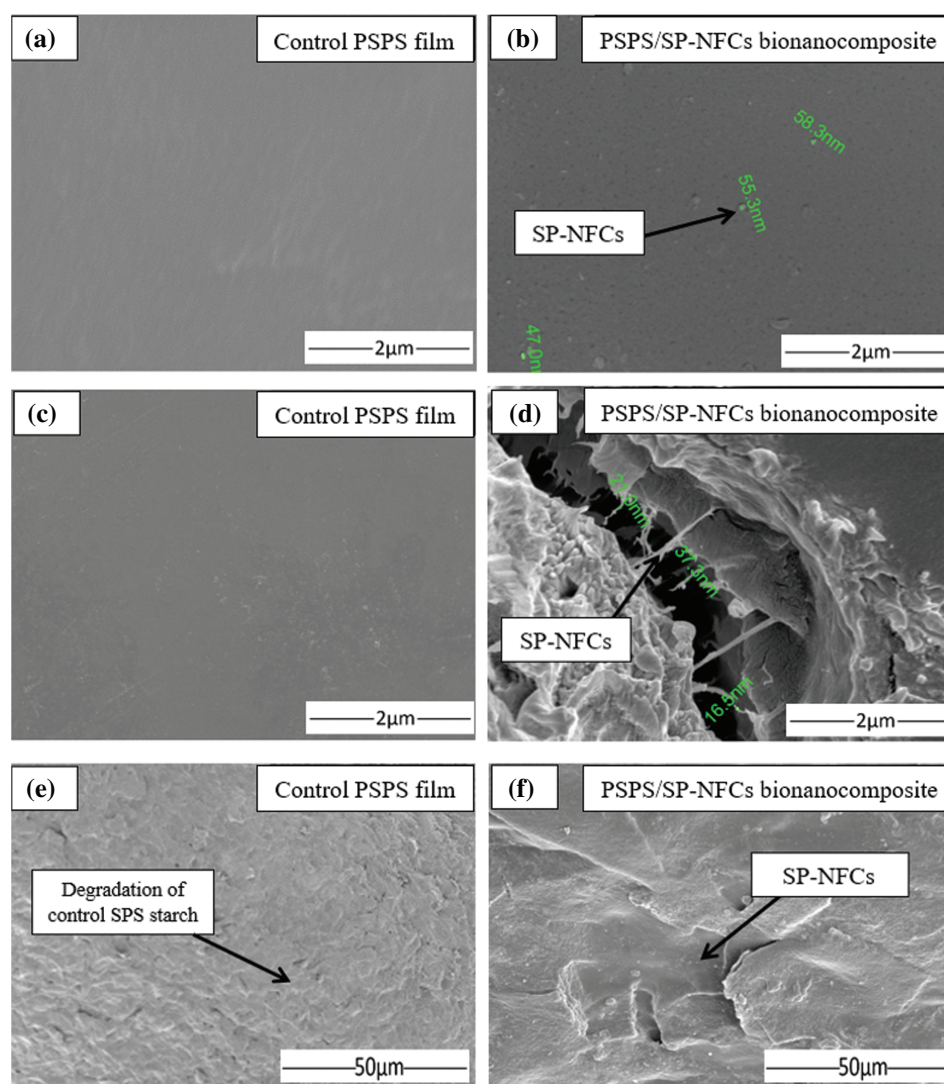


Fig. 5. FESEM micrographs of the outer and cross-sectional surfaces of samples after different exposition times to soil burial: (a) outer surface of control PSPS film before degradation; (b) outer surface of PSPS/SP-NFCs nanocomposite films before degradation; (c) cross-sectional surface of control PSPS film before degradation; (d) cross-sectional surface of PSPS/SP-NFCs nanocomposite films before degradation; (e) outer surface of PSPS/SP-NFCs nanocomposite films after 168 h; (f) cross-sectional surface of PSPS/SP-NFCs nanocomposite films after 168 h.

did not cause any severe deterioration/ ecological effects. In other words, the PSPS/SP-NFCs bio-nanocomposite films were completely biodegradable in the soil.

In order to visualise the morphological changes due to burial in soil, specimens of control PSPS film and PSPS/SP-NFCs bionanocomposite films were collected after being degraded in soil test for 168 h and FESEM micrographs were taken, as shown in Figure 5. At time zero, before the films being buried, the control PSPS film displayed a relatively smooth surface with some holes formed during the processing films (Fig. 5(a)). After 168 h, the decomposition was clearly observed for both films (Fig. 5(e)). The cracks and holes formed by soil bio-decomposition had random and uneven forms, as typically in material films decomposed in soils. The surface of the control films also became wavy and rough attributed to the attack by microorganisms within soil incubation. The deviations observed may be due to vacuum during sample sputtering for FESEM measurements. Before the PSPS/SP-NFCs nanocomposites were buried into the soil, they displayed a continuous surface with no trace of starch cracks or granular and agglomerations of SP-NFCs (Fig. 5(b)). After 168 h of soil burial, FESEM photographs revealed cracks and holes on the surface area of the PSPS/SP-NFCs nanocomposite films (Fig. 5(f)). SP-NFCs “noodle-like” nanofibres also seemed to be more visibly attributed to the loss of PSPS from the film. Besides, the effect of soil decomposition can be associated with weight loss of the bionanocomposites, as explained previously in Figure 4. The incorporation of SP-NFCs delayed the degradation of the PSPS/SP-NFCs bionanocomposite films. This phenomenon might be attributed to the high dispersion of SP-NFCs (Fig. 5(d)), which indicated a strong interfacial adhesion between the starch-based matrix and SP-NFCs nanofibre.

4. CONCLUSIONS

PSPS/SP-NFCs bio-nanocomposite films were fabricated by using solution casting technique. The PSPS/SP-NFCs bio-nanocomposite films possessed much higher thermal properties (DMA, TGA, DSC) than control starch due to the addition of nano-reinforcements which affected the segmental mobility of starch chains. DMA showed a marked improvement with the addition of SPNFC. Besides, as the content of SP-NFCs nanofillers increased in the PSPS polymer matrix, the resulting nanocomposites showed a higher water-resistance. The film water vapour permeability (WVP) of the PSPS/SP-NFCs bio-nanocomposite films was reduced with SP-NFCs nanofibres loading and was lower than control PSPS starch. The performance improvement of these PSPS/SP-NFCs bio-nanocomposites might be attributed to three-dimensional networks of intermolecular hydrogen bonding interactions between nanofiller and nanofiller and between

nanofillers and PSPS polymer; hence, making it lose its effectiveness in moisture permeability. The PSPS/SP-NFCs bio-nanocomposite films, consisting of biodegradable SP-NFCs and starch, are fully biodegradable, which are advantageous in terms of environmental protection and eco-friendly product.

Acknowledgments: The authors would like to thank Universiti Putra Malaysia and Ministry of Education, Malaysia for the financial support through the Graduate Research Fellowship (GRF) scholarship, Universiti Putra Malaysia Grant scheme Hi-CoE (6369107) and FRGS/1/2017/TK05/UPM/01/1 (5540048). The authors are grateful to Dr. Muhammed Lamin Sanyang for guidance throughout the experiment.

References

1. Sanyang, M.L., Ilyas, R.A., Sapuan, S.M. and Jumaidin, R., 2018. Sugar palm starch-based composites for packaging applications. in: *Bionanocomposites for Packaging Applications*. Cham, Springer International Publishing, pp.125–147.
2. Ilyas, R.A., Sapuan, S.M., Ishak, M.R. and Zainudin, E.S., 2018. Development and characterization of sugar palm nanocrystalline cellulose reinforced sugar palm starch bionanocomposites. *Carbohydrate Polymers*, 202, pp.186–202.
3. Halimatul, M.J., Sapuan, S.M., Jawaid, M., Ishak, M.R. and Ilyas, R.A., 2019. Effect of sago starch and plasticizer content on the properties of thermoplastic films: Mechanical testing and cyclic soaking-drying. *Polimery*, 64(6), pp.32–41.
4. Razali, N., Sapuan, S.M., Jawaid, M., Ishak, M.R. and Lazim, Y., 2016. Mechanical and thermal properties of roselle fibre reinforced vinyl ester composites. *BioResources*, 11(4), pp.9325–9339.
5. Sanyang, M.L., Sapuan, S.M., Jawaid, M., Ishak, M.R. and Sahari, J., 2016. Development and characterization of sugar palm starch and poly(lactic acid) bilayer films. *Carbohydrate Polymers*, 146, pp.36–45.
6. Kian, L.K., Jawaid, M., Ariffin, H. and Karim, Z., 2018. Isolation and characterization of nanocrystalline cellulose from roselle-derived microcrystalline cellulose. *International Journal of Biological Macromolecules*, 114, pp.54–63.
7. Kian, L.K., Jawaid, M., Ariffin, H. and Alothman, O.Y., 2017. Isolation and characterization of microcrystalline cellulose from roselle fibers. *International Journal of Biological Macromolecules*, 103, pp.931–940.
8. Ilyas, R.A., Sapuan, S.M., Ishak, M.R., Zainudin, E.S. and Atikah, M.S.N., 2018. Characterization of sugar palm nanocellulose and its potential for reinforcement with a starch-based composite. in: *Sugar Palm Biofibers, Biopolymers, and Biocomposites*. First edition. Boca Raton, FL, CRC Press/Taylor & Francis Group, CRC Press, pp.189–220.
9. El-Shekeil, Y.A., Salit, M.S., Abdan, K. and Zainudin, E.S., 2011. Development of a new kenaf bast fiber-reinforced thermoplastic polyurethane composite. *BioResources*, 6, pp.4662–4672.
10. Mansor, M.R., Sapuan, S.M., Zainudin, E.S., Nuraini, A.A. and Hambali, A., 2014. Conceptual design of kenaf fiber polymer composite automotive parking brake lever using integrated TRIZ-Morphological Chart-Analytic Hierarchy Process method. *Materials and Design*, 54, pp.473–482.
11. Jumaidin, R., Sapuan, S.M., Jawaid, M., Ishak, M.R. and Sahari, J., 2016. Characteristics of thermoplastic sugar palm starch/agar blend: Thermal, tensile, and physical properties. *International Journal of Biological Macromolecules*, 89, pp.575–581.

12. Abrial, H., Basri, A., Muhammad, F., Fernando, Y., Hafizulhaq, F., Mahardika, M., Sugiarti, E., Sapuan, S.M., Ilyas, R.A. and Stephane, I., **2019**. A simple method for improving the properties of the sago starch films prepared by using ultrasonication treatment. *Food Hydrocolloids*, 93, pp.276–283.
13. Abrial, H., Basri, A., Muhammad, F., Fernando, Y., Hafizulhaq, F., Mahardika, M., Sugiarti, E., Sapuan, S.M., Ilyas, R.A. and Stephane, I., **2019**. A simple method for improving the properties of the sago starch films prepared by using ultrasonication treatment. *Food Hydrocolloids*, 93, pp.276–283.
14. Halimatul, M.J., Sapuan, S.M., Jawaid, M., Ishak, M.R. and Ilyas, R.A., **2019**. Water absorption and water solubility properties of sago starch biopolymer composite films filled with sugar palm particles. *Polimery*, 64(9), pp.27–35.
15. Sanyang, M.L., Sapuan, S.M., Jawaid, M., Ishak, M.R. and Sahari, J., **2016**. Effect of sugar palm-derived cellulose reinforcement on the mechanical and water barrier properties of sugar palm starch biocomposite films. *BioResources*, 11(2), pp.4134–4145.
16. Sapuan, S.M., Ilyas, R.A., Ishak, M.R., Leman, Z., Huzaifah, M.R.M., Ammar, I.M. and Atikah, M.S.N., **2018**. Development of sugar palm-based products: A community project. in: *Sugar Palm Biofibers, Biopolymers, and Biocomposites*. First edition. Boca Raton, FL, CRC Press/Taylor & Francis Group, CRC Press, pp.245–266.
17. Ilyas, R.A., Sapuan, S.M., Ishak, M.R. and Zainudin, E.S., **2018b**. Water transport properties of bio-nanocomposites reinforced by sugar palm (*Arenga Pinnata*) nanofibrillated cellulose. *Journal of Advanced Research in Fluid Mechanics and Thermal Sciences Journal*, 51(2), pp.234–246.
18. Ilyas, R.A., Sapuan, S.M., Ishak, M.R., Zainudin, E.S. and Atikah, M.S.N., **2018**. Nanocellulose Reinforced Starch Polymer Composites: A Review of Preparation, Properties and Application. *Proceeding: 5th International Conference on Applied Sciences and Engineering (ICASEA, 2018)*. Hotel, Capthorne Cameron Highlands, Malaysia, pp.325–341.
19. Ilyas, R.A., Sapuan, S.M., Ishak, M.R., Zainudin, E.S., Atikah, M.S.N. and Huzaifah, M.R.M., **2018b**. Water barrier properties of biodegradable films reinforced with nanocellulose for food packaging application: A review. *6th Postgraduate Seminar on Natural Fiber Reinforced Polymer Composites 2018*. Serdang, Selangor, pp.55–59.
20. Kaushik, A., Singh, M. and Verma, G., **2010**. Green nanocomposites based on thermoplastic starch and steam exploded cellulose nanofibrils from wheat straw. *Carbohydrate Polymers*, 82(2), pp.337–345.
21. Ilyas, R.A., Sapuan, S.M., Sanyang, M.L., Ishak, M.R. and Zainudin, E.S., **2018**. Nanocrystalline cellulose as reinforcement for polymeric matrix nanocomposites and its potential applications: A review. *Current Analytical Chemistry*, 14(3), pp.203–225.
22. Ilyas, R.A., Sapuan, S.M., Ishak, M.R. and Zainudin, E.S., **2018c**. Sugar Palm Nanocrystalline Cellulose Reinforced Sugar Palm Starch Composite: Degradation and Water-Barrier Properties. *IOP Conference Series: Materials Science and Engineering*.
23. Ilyas, R.A., Sapuan, S.M. and Ishak, M.R., **2018**. Isolation and characterization of nanocrystalline cellulose from sugar palm fibres (*Arenga Pinnata*). *Carbohydrate Polymers*, 181, pp.1038–1051.
24. Abdul Khalil, H.P.S., Bhat, A.H. and Yusra, A.F.I., **2012**. Green composites from sustainable cellulose nanofibrils: A review. *Carbohydrate Polymers*, 87(2), pp.963–979.
25. Ilyas, R.A., Sapuan, S.M., Ibrahim, R., Abrial, H., Ishak, M.R., Zainudin, E.S., Asrofi, M., Atikah, M.S.N., Huzaifah, M.R.M., Radzi, A.M., Azammi, A.M.N., Shaharuzaman, M.A., Nurazzi, N.M., Syafri, E., Sari, N.H., Norrahim, M.N.F. and Jumaidin, R., **2019**. Sugar palm (*Arenga pinnata* (Wurmb.) Merr) cellulosic fibre hierarchy: A comprehensive approach from macro to nano scale. *Journal of Materials Research and Technology*, 8(3), pp.2753–2766.
26. Pelissari, F.M., Andrade-Mahecha, M.M., Sobral, P.J. do A. and Menegalli, F.C., **2017**. Nanocomposites based on banana starch reinforced with cellulose nanofibers isolated from banana peels. *Journal of Colloid and Interface Science*, 505, pp.154–167.
27. Lu, P. and Hsieh, Y., **2012**. Preparation and characterization of cellulose nanocrystals from rice straw. *Carbohydrate Polymers*, 87(1), pp.564–573.
28. Dufresne, A., Cavallé, J.-Y. and Helbert, W., **1997**. Thermoplastic nanocomposites filled with wheat straw cellulose whiskers. Part II: Effect of processing and modeling. *Polymer Composites*, 18(2), pp.198–210.
29. Flauzino Neto, W.P., Silvério, H.A., Dantas, N.O. and Pasquini, D., **2013**. Extraction and characterization of cellulose nanocrystals from agro-industrial residue–Soy hulls. *Industrial Crops and Products*, 42, pp.480–488.
30. Rosa, M.F.M., Medeiros, E.S., Malmonge, J.A.J., Gregorski, K.S., Wood, D.F., Mattoso, L.H.C., Glenn, G., Orts, W.J. and Imam, S.H., **2010**. Cellulose nanowhiskers from coconut husk fibers: Effect of preparation conditions on their thermal and morphological behavior. *Carbohydrate Polymers*, 81(1), pp.83–92.
31. Sheltami, R.M., Abdullah, I., Ahmad, I., Dufresne, A. and Kargarzadeh, H., **2012**. Extraction of cellulose nanocrystals from mengkuang leaves (*Pandanus tectorius*). *Carbohydrate Polymers*, 88(2), pp.772–779.
32. Teixeira, E. de M., Bondancia, T.J., Teodoro, K.B.R., Corrêa, A.C., Marconcini, J.M. and Mattoso, L.H.C., **2011**. Sugarcane bagasse whiskers: Extraction and characterizations. *Industrial Crops and Products*, 33(1), 63–66.
33. Cherian, B.M., Leão, A.L., de Souza, S.F., Thomas, S., Pothan, L.A. and Kottaisamy, M., **2010**. Isolation of nanocellulose from pineapple leaf fibres by steam explosion. *Carbohydrate Polymers*, 81(3), pp.720–725.
34. Huzaifah, M.R.M., Sapuan, S.M., Leman, Z., Ishak, M.R. and Maleque, M.A., **2017**. A review of sugar palm (*Arenga pinnata*): Application, fibre characterisation and composites. *Multidiscipline Modeling in Materials and Structures*, 13(4), pp.678–698.
35. Ammar, I.M., Huzaifah, M.R.M., Sapuan, S.M., Ishak, M.R. and Leman, Z.B., **2018**. Development of sugar palm fiber reinforced vinyl ester composites. *Natural Fibre Reinforced Vinyl Ester and Vinyl Polymer Composites*. Elsevier, pp.211–224.
36. Radzi, A.M., Sapuan, S.M., Jawaid, M. and Mansor, M.R., **2017**. Influence of fibre contents on mechanical and thermal properties of roselle fibre reinforced polyurethane composites. *Fibers and Polymers*, 18(7), pp.1353–1358.
37. Jumaidin, R., Sapuan, S.M., Jawaid, M., Ishak, M.R. and Sahari, J., **2016**. Effect of seaweed on physical properties of thermoplastic sugar palm starch/agar composites. *Journal of Mechanical Engineering and Sciences*, 10(3), pp.2214–2225.
38. Mazani, N., Sapuan, S.M., Sanyang, M.L., Atiqah, A. and Ilyas, R.A., **2019**. Design and fabrication of a shoe shelf from Kenaf fiber reinforced unsaturated polyester composites. in: *Lignocellulose for Future Bioeconomy*. Elsevier, pp.315–332.
39. Sapuan, S.M. and Ilyas, R.A., **2017**. Sugar palm: Fibers, biopolymers and biocomposites. *INTROPica*, pp.5–7.
40. Sapuan, S.M., Ishak, M.R., Leman, Z., Ilyas, R.A. and Huzaifah, M.R.M., **2017**. Development of products from sugar palm trees (*Arenga Pinnata* Wurb. Merr): A community project. *INTROPica*, pp.12–13.
41. Sanyang, M.L., Sapuan, S.M., Jawaid, M., Ishak, M.R. and Sahari, J., **2016**. Recent developments in sugar palm (*Arenga pinnata*) based biocomposites and their potential industrial applications: A review. *Renewable and Sustainable Energy Reviews*, 54, pp.533–549.
42. Bachtiar, D., Sapuan, S.M. and Hamdan, M.M., **2010**. Flexural properties of alkaline treated sugar palm fibre reinforced epoxy composites. *International Journal of Automotive and Mechanical Engineering*, 1(1), pp.79–90.

43. Sahari, J., Sapuan, S.M., Zainudin, E.S. and Maleque, M.A., **2013b**. Effect of water absorption on mechanical properties of sugar palm fibre reinforced sugar palm starch (SPF/SPS) biocomposites. *Journal of Biobased Materials and Bioenergy*, 7(1), pp.90–94.
44. Ishak, M.R., Leman, Z., Sapuan, S.M., Salleh, M.Y. and Misri, S., **2009**. Effect of sea water treatment on the impact and flexural strength of sugar palm fibre reinforced epoxy composites. *International Journal of Mechanical and Materials Engineering (IJMME)*, 4(3), pp.316–320.
45. Sahari, J., Salit, M.S., Zainudin, E.S. and Maleque, M.A., **2014**. Degradation Characteristics of SPF/SPS biocomposites fabrication of SPF/SPS biocomposites. *Fibres and Textiles in Eastern Europe*, 22(5107), pp.96–98.
46. Ilyas, R.A., Sapuan, S.M., Ishak, M.R. and Zainudin, E.S., **2017**. Effect of delignification on the physical, thermal, chemical, and structural properties of sugar palm fibre. *BioResources*, 12(4), pp.8734–8754.
47. ASTM D1104-56, **1978**. *Method of Test for Holocellulose in Wood*. USA, American Society for Testing and Materials.
48. ASTM D1103-60, **1977**. *Method of Test for Alpha-Cellulose in Wood*. USA, American Society for Testing and Materials.
49. ISO 5264-2, **2002**. Pulps—Laboratory beating—Part 2: PFI mill method.
50. Ferrer, A., Filpponen, I., Rodríguez, A., Laine, J. and Rojas, O.J., **2012**. Valorization of residual empty palm fruit bunch fibers (EPFBF) by microfluidization: Production of nanofibrillated cellulose and EPFBF nanopaper. *Bioresource Technology*, 125, pp.249–255.
51. Radzi, A.M., Sapuan, S.M., Jawaid, M. and Mansor, M.R., **2018**. Mechanical performance of roselle/sugar palm fiber hybrid reinforced polyurethane composites. *BioResources*, 13(3), pp.6238–6249.
52. ASTM D5026-15, **2015**. Standard Test Method for Plastics: Dynamic Mechanical Properties: In Tension.
53. ASTM E 95-96, **1995**. Standard Test Methods for Water Vapor Transmission of Materials.
54. Edhirej, A., Sapuan, S.M., Jawaid, M. and Zahari, N.I., **2017**. Preparation and characterization of cassava bagasse reinforced thermoplastic cassava starch. *Fibers and Polymers*, 18(1), pp.162–171.
55. Sanyang, M.L., Sapuan, S.M., Jawaid, M., Ishak, M.R. and Sahari, J., **2015**. Effect of plasticizer type and concentration on dynamic mechanical properties of sugar palm starch-based films. *International Journal of Polymer Analysis and Characterization*, 20(7), pp.627–636.
56. Sahari, J., Sapuan, S.M., Zainudin, E.S. and Maleque, M.A., **2013c**. Thermo-mechanical behaviors of thermoplastic starch derived from sugar palm tree (*Arenga pinnata*). *Carbohydrate Polymers*, 92(2), pp.1711–1716.
57. Zhong, Y. and Li, Y., **2014**. Effects of glycerol and storage relative humidity on the properties of kudzu starch-based edible films. *Starch/Staerke*, 66(5–6), pp.524–532.
58. Jumaidin, R., Sapuan, S.M., Jawaid, M., Ishak, M.R. and Sahari, J., **2017b**. Thermal, mechanical, and physical properties of seaweed/sugar palm fibre reinforced thermoplastic sugar palm Starch/Agar hybrid composites. *International Journal of Biological Macromolecules*, 97, pp.606–615.
59. Jumaidin, R., Sapuan, S., Jawaid, M., Ishak, M. and Sahari, J., **2017a**. Effect of agar on flexural, impact, and thermogravimetric properties of thermoplastic sugar palm starch. *Current Organic Synthesis*, 14(2), pp.200–205.
60. Silvério, H.A., Flauzino Neto, W.P., Dantas, N.O. and Pasquini, D., **2013**. Extraction and characterization of cellulose nanocrystals from corn cob for application as reinforcing agent in nanocomposites. *Industrial Crops and Products*, 44, pp.427–436.
61. Chen, Y., Liu, C., Chang, P.R., Cao, X. and Anderson, D.P., **2009**. Bionanocomposites based on pea starch and cellulose nanowhiskers hydrolyzed from pea hull fibre: Effect of hydrolysis time. *Carbohydrate Polymers*, 76(4), pp.607–615.
62. Li, W., Yue, J. and Liu, S., **2012**. Preparation of nanocrystalline cellulose via ultrasound and its reinforcement capability for poly(vinyl alcohol) composites. *Ultrasonics Sonochemistry*, 19(3), pp.479–485.
63. Anglès, M.N. and Dufresne, A., **2000**. Plasticized starch/tunicin whiskers nanocomposites. 1. Structural analysis. *Macromolecules*, 33(22), pp.8344–8353.
64. Savadekar, N.R. and Mhaske, S.T., **2012**. Synthesis of nano cellulose fibers and effect on thermoplastics starch based films. *Carbohydrate Polymers*, 89(1), pp.146–151.
65. Lu, Y., Weng, L. and Cao, X., **2005**. Biocomposites of plasticized starch reinforced with cellulose crystallites from cottonseed linter. *Macromolecular Bioscience*, 5(11), pp.1101–1107.
66. Balakrishnan, P., Sreekala, M.S., Kunaver, M., Huskić, M. and Thomas, S., **2017**. Morphology, transport characteristics and viscoelastic polymer chain confinement in nanocomposites based on thermoplastic potato starch and cellulose nanofibers from pineapple leaf. *Carbohydrate Polymers*, 169, pp.176–188.
67. Oommen, Z., Groeninckx, G. and Thomas, S., **2000**. Dynamic mechanical and thermal properties of physically compatibilized natural rubber/poly(methyl methacrylate) blends by the addition of natural rubber-graft- poly(methyl methacrylate). *Journal of Polymer Science Part B: Polymer Physics*, 38(4), pp.525–536.
68. Einstein, A., **1956**. Investigations on the theory of brownian motion.
69. Abdalla, F.H., Megat, M.H., Sapuan, M.S. and Sahari, B.B., **2008**. Determination of volume fraction values of filament wound glass and carbon fiber reinforced composites. *ARPN Journal of Engineering and Applied Sciences*, 3(4), pp.7–11.
70. George, J., Ramana, K. V., Bawa, A.S. and Siddaramaiah, **2011**. Bacterial cellulose nanocrystals exhibiting high thermal stability and their polymer nanocomposites. *International Journal of Biological Macromolecules*, 48(1), pp.50–57.
71. Noshirvani, N., Ghanbarzadeh, B., Fasihi, H. and Almasi, H., **2016**. Starch-PVA nanocomposite film incorporated with cellulose nanocrystals and MMT: A comparative study. *International Journal of Food Engineering*, 12(1), pp.37–48.
72. Wilhelm, H.M., Sierakowski, M.R., Souza, G.P. and Wypych, F., **2003**. Starch films reinforced with mineral clay. *Carbohydrate Polymers*, 52(2), pp.101–110.
73. Slavutsky, A.M. and Bertuzzi, M.A., **2014**. Water barrier properties of starch films reinforced with cellulose nanocrystals obtained from sugarcane bagasse. *Carbohydrate Polymers*, 110, pp.53–61.
74. Follain, N., Belbekhouche, S., Bras, J., Siqueira, G., Marais, S. and Dufresne, A., **2013**. Water transport properties of bio-nanocomposites reinforced by *Luffa cylindrica* cellulose nanocrystals. *Journal of Membrane Science*, 427, pp.218–229.
75. Masclaux, C., Gouanvé, F. and Espuche, E., **2010**. Experimental and modelling studies of transport in starch nanocomposite films as affected by relative humidity. *Journal of Membrane Science*, 363(1–2), pp.221–231.
76. Tahri, N., Bahafid, W., Sayel, H. and El Ghachtouli, N., **2013**. Biodegradation: Involved microorganisms and genetically engineered microorganisms. in: *Biodegradation—Life of Science*. InTech. pp.289–320.
77. Kiatkamjornwong, S., Sonsuk, M., Wittayapichet, S., Prasarakich, P. and Vejjanukroh, P.-C., **1999**. Degradation of styrene-g-cassava starch filled polystyrene plastics. *Polymer Degradation and Stability*, 66(3), pp.323–335.
78. Wan, Y.Z., Luo, H., He, F., Liang, H., Huang, Y. and Li, X.L., **2009**. Mechanical, moisture absorption, and biodegradation behaviours of bacterial cellulose fibre-reinforced starch biocomposites. *Composites Science and Technology*, 69(7–8), pp.1212–1217.
79. Ilyas, R.A., Sapuan, S.M., Ishak, M.R. and Zainudin, E.S., **2019**. Sugar palm nanofibrillated cellulose (*Arenga pinnata* (Wurmb.)

- Merr*): Effect of cycles on their yield, physic-chemical, morphological and thermal behavior. *International Journal of Biological Macromolecules*, 123, pp.379–388.
80. Fan, L.T., Lee, Y.-H. and Beardmore, D.H., 1980. Mechanism of the enzymatic hydrolysis of cellulose: Effects of major structural features of cellulose on enzymatic hydrolysis. *Biotechnology and Bioengineering*, 22(1), pp.177–199.
81. Alvarez, V.A., Ruseckaite, R.A. and Vázquez, A., 2006. Degradation of sisal fibre/Mater Bi-Y biocomposites buried in soil. *Polymer Degradation and Stability*, 91(12), pp.3156–3162.
82. Żuchowska, D., Steller, R. and Meissner, W., 1998. Structure and properties of degradable polyolefin-starch blends. *Polymer Degradation and Stability*, 60(2–3), pp.471–480.

Received: 6 December 2018. Accepted: 17 June 2019.